Journal of Power Sources 205 (2012) 122–128

Contents lists available at SciVerse ScienceDirect

Journal of Power Sources

journal homepage: www.elsevier.com/locate/jpowsour

$Gd_{0.1}Ce_{0.9}O_{1.95}/Er_{0.4}Bi_{1.6}O_3$ bilayered electrolytes fabricated by a simple colloidal route using nano-sized $Er_{0.4}Bi_{1.6}O_3$ powders for high performance low temperature solid oxide fuel cells

Kang Taek Lee[a,b], Doh Won Jung[c], Matthew A. Camaratta[b], Hee Sung Yoon[a], Jin Soo Ahn[d], Eric D. Wachsman[a,*]

[a] University of Maryland Energy Research Center, University of Maryland, College Park, MD 20742, USA
[b] Department of Materials Science and Engineering, University of Florida, Gainesville, FL 32611, USA
[c] Samsung Advanced Institute of Technology, Yongin-si, Republic of Korea
[d] Research Institute of Industrial Science and Technology, Pohang, Republic of Korea

ARTICLE INFO

Article history:
Received 1 November 2011
Received in revised form
20 December 2011
Accepted 1 January 2012
Available online 10 January 2012

Keywords:
Electrolyte
Bilayer
Stabilized bismuth oxide
Co-precipitation
Solid oxide fuel cells
LT-SOFC

ABSTRACT

Thin and dense bilayer electrolytes consisting of erbium stabilized bismuth oxide (ESB) and gadolinium-doped ceria (GDC) were fabricated on tape-cast porous Ni–GDC anode-supports using a scalable and cost-effective colloidal deposition process. Nano-sized ESB particles were successfully synthesized at temperatures as low as ~500 °C using wet chemical co-precipitation. Due to the high sinterability of this powder, dense ESB layers were obtained at a sintering temperature of 800 °C. Scanning electron microscopy and energy-dispersive X-ray spectroscopy analysis of a full button cell with an ESB/GDC bilayer sintered at 800 °C showed no visible interfacial diffusion between each layer. A systematic study on the sintering behavior of ESB revealed that at higher sintering temperatures, bismuth oxide can sublime or penetrate into the GDC sublayer. The effect of both the ESB layer and the GDC layer thickness on increasing open circuit potential (OCP) was demonstrated. The current–voltage measurement of the cell showed high power density (~1.5 W cm^{-2}) at 650 °C due to the increase in OCP and a significant reduction in area specific resistance when compared to solid oxide fuel cells (SOFCs) with a single GDC layer. These results demonstrate that ESB/GDC bilayer electrolytes have significant potential for high performance SOFCs at low operational temperature.

© 2012 Elsevier B.V. All rights reserved.

1. Introduction

Solid oxide fuel cells (SOFCs) have been widely studied as a next-generation energy conversion device. They produce electricity by electrochemically reacting fuel and oxidant separated by a ceramic ionic conductor, i.e., a solid state electrolyte [1]. The efficiency of SOFCs is not limited by the Carnot cycle of combustion-type systems, and can reach approximately 45–60%. Considering utilization of the by-product heat in co-generation or bottoming cycles, the projected system efficiency can exceed 80%. In addition to high efficiency, SOFCs are attractive because they do not produce NO_x, and have significantly lower green house gas emissions compared to combustion engines.

High system cost is one of the largest barriers to the commercialization of SOFC technology. Lower temperature operation (<700 °C) can significantly reduce the system cost by allowing the use of inexpensive steel for the bipolar plates and balance-of-plant, and the use of high temperature gaskets rather than rigid glass-based seals, further enhancing mechanical stability and lifetime [2].

However, the reduced oxygen ion conduction in ceramic electrolytes results in a significant increase in ohmic polarization at low temperatures (LT, <700 °C). Therefore, development of higher conductivity electrolytes has been investigated by many researchers [2,3].

Among the studied electrolyte materials, doped-ceria and stabilized bismuth oxide have 1–2 orders of magnitude higher ionic conductivity than conventional yttria stabilized zirconia (YSZ) electrolytes [4]. However, doped ceria is a mixed ionic electronic conductor (MIEC) exhibiting a lower open circuit potential (OCP) than the theoretical Nernst voltage due to electronic leakage, which results in lower power density and efficiency [5]. Moreover, although stabilized bismuth oxide has very high oxygen ionic conductivity, its inherent thermodynamic instability under reducing conditions makes it a poor choice by itself as an electrolyte for SOFCs [6].

* Corresponding author at: Engineering Lab Bldg., University of Maryland, College Park, MD 20742, USA. Tel.: +1 301 405 8193; fax: +1 301 314 8514.
E-mail address: ewach@umd.edu (E.D. Wachsman).

0378-7753/$ – see front matter © 2012 Elsevier B.V. All rights reserved.
doi:10.1016/j.jpowsour.2012.01.040

To overcome these problems, Wachsman et al. suggested a bismuth oxide/ceria bilayer electrolyte consisting of a layer of stabilized bismuth oxide on the oxidizing side and a layer of doped ceria on the reducing side to improve the thermodynamic stability of the bismuth oxide layer, by shielding it from very low Po_2, and to block electronic flux from doped ceria in reducing atmospheres [7]. A number of studies have demonstrated that the OCP can be effectively improved using the bismuth oxide/ceria bilayered electrolyte concept [7–10]. Previously, Park et al. reported that an ultra thin (~0.2 μm) and dense ESB layer can be deposited on Sm-doped ceria (SDC) pellets by pulsed laser deposition (PLD) [8,9]. In addition, to overcome the reactivity of ESB with conventional perovskite cathodes, a bismuth ruthenate ($Bi_2Ru_2O_7$, BRO7)–ESB composite cathode was developed [11]. A recent optimization study by Camaratta and Wachsman reported that BRO7–ESB composite cathodes exhibited very low ASR (0.73 and 0.03 Ω cm^2 at 500 and 700 °C, respectively) [12].

Based on these studies, we demonstrated ~1.94 W cm^{-2} at 650 °C using a thin ESB/GDC electrolyte on an anode-supported cell with BRO7–ESB cathodes [13,14]. In this study, thin (~4 μm) and relatively dense ESB was successfully deposited by PLD on 10 μm thick GDC film. One of the key factors to fabricating ESB/GDC bilayered electrolytes is to obtain a dense and thin ESB layer on the sintered GDC electrolyte. Although PLD is good for demonstration purposes in lab-scale experiments, a more cost-effective and scalable fabrication process is necessary for future application of the ESB/GDC bilayered electrolyte.

In this study, we fabricated thin and dense ESB/GDC bilayered electrolytes on tape-cast porous Ni–GDC anode-supports by a simple and cost-effective colloidal deposition process. To obtain a dense ESB layer, nano-sized ESB particles used for the colloidal coating slurry were synthesized by wet chemical coprecipitation. In order to optimize the sintering conditions of the ESB layer on dense GDC, the evolution of the ESB microstructure with sintering temperature was investigated. Moreover, the effect of total and relative thickness of ESB/GDC bilayered electrolytes on OCP was determined. In addition, current–voltage and electrochemical impedance measurements were used to determine SOFC performance.

2. Experimental procedure

2.1. ESB powder fabrication

Coprecipitation was employed to synthesize nano-scale ESB ($Er_{0.4}Bi_{1.6}O_3$) powder. Pure $Bi(NO_3)_3{\cdot}5H_2O$ (Alfa Aesar) and $Er(NO_3)_3{\cdot}5H_2O$ (Alfa Aesar) were used as starting materials. They were weighed in stoichiometric proportions and dissolved in 70% HNO_3 to produce a solution with 0.125 M metal ion concentration (pH 0). Ammonium hydroxide (Acros Organics, 28–30% of NH_3 in water) was added dropwise to the stirred solution to increase the pH value to 12. The solution was maintained at 80 °C during the coprecipitation. The addition of the ammonia solution resulted in the formation of a pale pink color precipitate. The precipitate was vacuum-filtered and washed with DI-water in a Buchner funnel. Subsequently, the washed powder was dried at 80 °C for 12 h. The agglomerated powder was then ground into fine particles using a mortar and pestle. The powder was calcined at 500 °C for 4 h in air.

For comparison purposes, ESB powder was synthesized by the conventional solid-state route (ss-ESB). A stoichiometric mixture of Bi_2O_3 (99.9995% pure) and Er_2O_3 (99.99% pure), from Alfa Aesar, were mixed and ball-milled with YSZ ball media (Advanced Materials) in ethanol in a high-density polyethylene bottle for 24 h. After drying, the mixed powders of ESB were calcined at 800 °C for 16 h. Agglomerated powders were ground using mortar and pestle and sieved using a 325 μm mesh.

2.2. Fuel cell fabrication

SOFC fabrication involved spin coating GDC on tape-cast NiO–GDC anodes followed by ESB colloidal drop coating. The anode support was prepared by tapecasting a slurry of 65 wt% NiO (Alfa Aesar) and 35 wt% GDC (Rhodia) in an organic solvent/binder system. Anode tapes were presintered at 900 °C for 2 h and a GDC anode functional layer (AFL) was deposited by spraying the GDC precursor solution on the presintered anode surface. Detailed preparation and fabrication of GDC AFL on tape-cast anodes was previously described [15].

Thin and uniform GDC electrolytes were deposited by spin coating the colloidal GDC slurry. Rhodia GDC powder was ball milled for 24 h with 1 wt% Solsperse (dispersant) in ethanol. After the first ball-milling step, 10 wt% PVB (binder) and 2 wt% DBP (plasticizer) were added and the solution was ball-milled for an additional 24 h. The anode substrates were then spin coated with the slurry. The GDC electrolyte thickness was controlled by the number of coatings at the same spin speed. Between the coatings, the applied layer was allowed to dry for 20 min at room temperature. Samples were then dried at room temperature for 10 h. After drying, the GDC-electrolyte/anode structure was sintered at 1450 °C for 4 h using a ramp rate of 3 °C min^{-1} in air.

For the ESB/GDC bilayered electrolytes, the ESB layer was deposited by drop coating co-precipitated ESB (cp-ESB) and ss-ESB colloidal slurries. To make the ESB colloidal slurry cp-ESB powder was mixed with a binder system consisting of 1 wt% Solsperse, 2 wt% DBP and 10 wt% PVB as the dispersant, plasticizer, and binder, respectively. This mixture was ball-milled in ethanol for 24 h, drop-coated onto the sintered GDC electrolyte surface, and dried for 30 min. The drop-coating was repeated until a desired thickness was achieved.

To determine the effect of sintering temperature on ESB layer formation, an as-deposited ESB/GDC bilayered cell was divided into several pieces with a diamond saw and the pieces sintered at 700, 800, and 900 °C for 4 h using a 400 °C 1 h binder burnout step, and a 5 °C min^{-1} ramp rate. For comparison, the same experiments were repeated using ss-ESB powder.

Two different composite cathodes were used for this study – LSCF-GDC (50:50 wt%) on the GDC electrolyte and BRO7–ESB (50:50 wt%) on the ESB/GDC bilayered electrolytes. This is necessary since LSCF reacts with ESB so we cannot use it on the bilayered electrolyte cells, and the use of BRO7–ESB cathodes invariably results in the formation of an ESB layer on the GDC surface, thus masking single layer GDC OCP results. For the BRO7–ESB cathode both powders were synthesized by conventional solid-state route. The cathode development and deposition procedure can be found in earlier work [12,14].

2.3. Characterization

The phase and size of the crystallites of as-calcined ESB powders were investigated by X-ray diffraction analysis (XRD, Philips APD 3720). Microstructures of ESB powders and fuel cell structures with ESB/GDC bilayered electrolytes were observed using scanning electron microscopy (SEM, JEOL 6400/6335F). Qualitative elemental analysis of the fuel cell structure was conducted by energy-dispersive X-ray spectroscopy (EDX).

For electrochemical performance measurement, SOFC samples were loaded in a fuel cell test station. The SOFC edge was sealed to the testing alumina tube using a Ceramabond-517 two-part, liquid and powder, mixture (Aremco). OCP measurements and current–voltage (I–V) characteristics were conducted by a Solartron

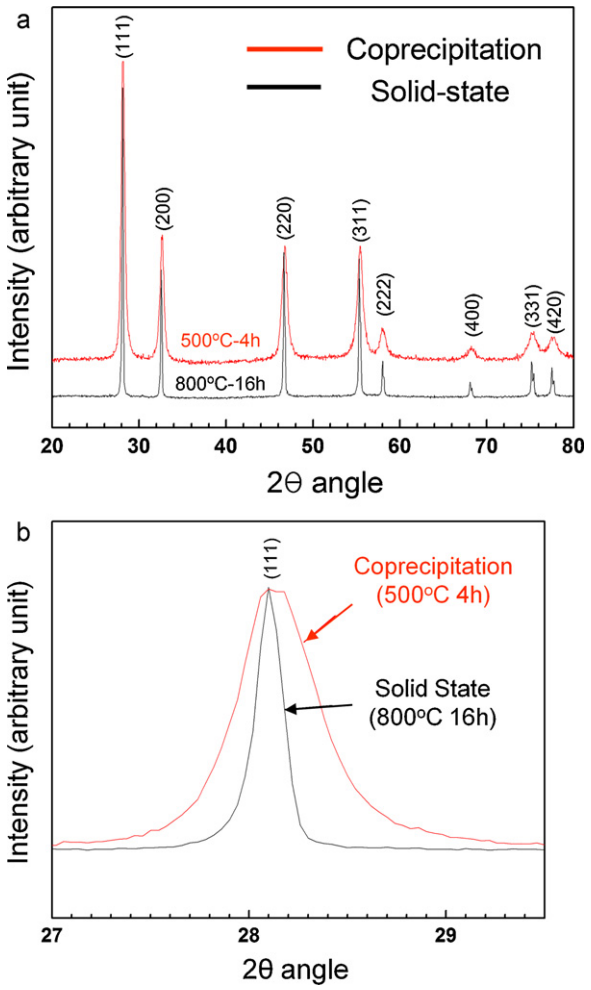

Fig. 1. XRD diffraction patterns of ESB powders synthesized by coprecipitation route (red line) and solid state route (black line) (a). The magnified XRD diffraction pattern of the (1 1 1) peak is shown at the 2θ range from 27 to 29° (b). (For interpretation of the references to color in this figure legend, the reader is referred to the web version of the article.)

1287 potentiostat under gas conditions of dry air and 3% wet hydrogen to the cathode and anode side, respectively. After the *I–V* measurement, two-point probe impedance analysis was carried out under open circuit condition using a Par-stat 2273 (Princeton Applied Research) over a frequency range of 100 kHz to 100 mHz with ac signal strength of 50 mV.

3. Results and discussion

3.1. Powder characterization

Fig. 1 shows the XRD results of ESB powders synthesized by co-precipitation and solid-state routes. For cp-ESB, the precursor powder was calcined at 500 °C for 4 h, while ss-ESB powder was calcined at 800 °C for 16 h (typical temperature for ESB [16]). As shown in Fig. 1a, both cp-ESB and ss-ESB exhibit the doped-bismuth oxide cubic-fluorite structure without any secondary phases. This indicates that co-precipitation synthesis of ESB powder is an effective way to reduce the calcination temperature and processing time compared to the conventional solid-state route.

The crystallite size of the material was calculated by the Scherrer equation [17]:

$$B(2\theta) = \frac{K\lambda}{L\cos\theta} \quad (1)$$

Table 1
Calcination condition and crystallite size of ESB powders synthesis by co-precipitation and solid state route.

Synthesis route	Calcine condition	FWHM (°, 2θ)	Crystallite size (Å)
Co-precipitation	500 °C for 4 h	0.48	171
Solid state	800 °C for 16 h	0.16	512

where K is the shape factor, λ is the X-ray wavelength, typically 1.54 Å, B is the line broadening at half the maximum intensity (FWHM) in radians, θ is the Bragg angle, and L is the crystallite length. Fig. 1b shows the magnified X-ray diffraction pattern of the (1 1 1) peak from Fig. 1a at the 2-theta range from 27° to 29°. The calculated crystallite sizes of both ESB powders by Eq. (1) are summarized in Table 1. The crystallite size of cp-ESB was 1/3 that of ss-ESB, indicating smaller particle sizes for cp-ESB powder due to the lower thermal energy input during cubic-fluorite phase formation.

SEM images of the ESB powders prepared from the different synthesis methods are shown in Fig. 2. The cp-ESB powder are highly porous particulates (less than 1–3 μm) consisting of agglomerations of nano-sized rods (less than 100 nm) (Fig. 2a). In contrast, the ss-ESB powder shows hard particles over ~5 μm in size (Fig. 2b). Based on a Brunauer–Emmett–Teller (BET) method, the surface area (S) of a material can be estimated using a general formula written as;

$$S = 6\frac{V}{d} \quad (2)$$

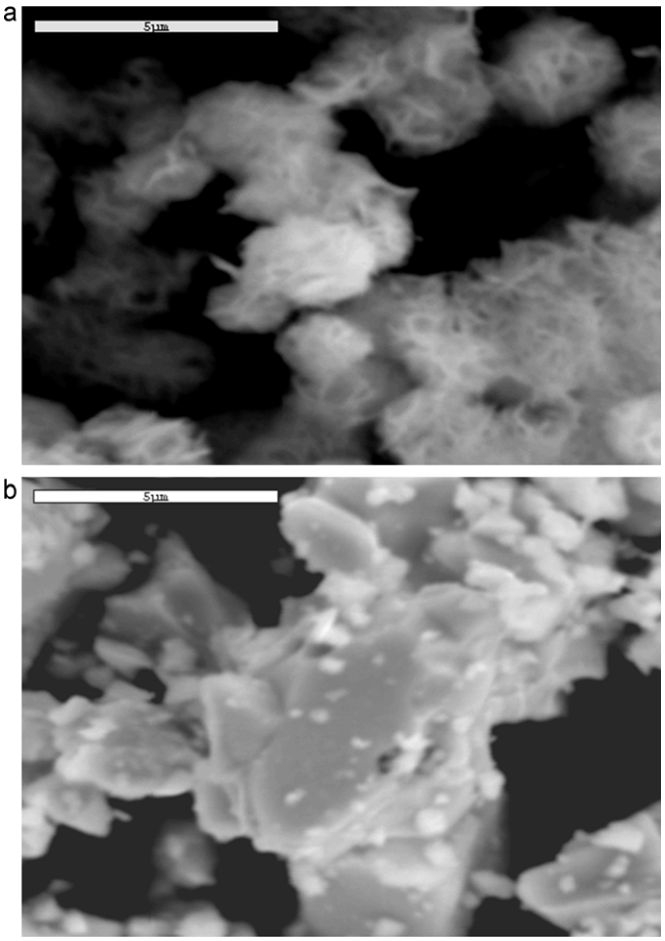

Fig. 2. SEM of ESB powders synthesized by wet-chemical co-precipitation method (a) and solid-state route (b).

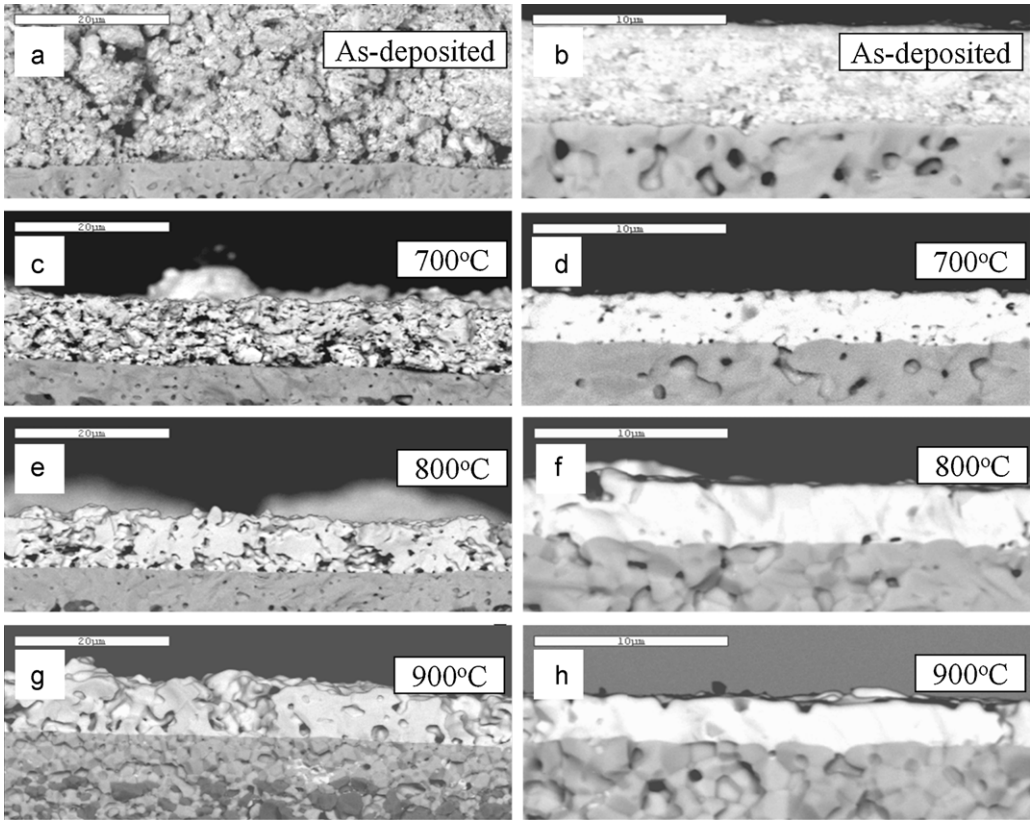

Fig. 3. Evolution of ESB layers on GDC electrolyte at various sintering temperatures using ss-ESB (a, c, e, and g) and cp-ESB (b, d, f, and h). It is noted that the magnification of images for ESB electrolyte using cp-ESB powder is higher that that of ss-ESB powder.

where V and d are the volume and effective particle diameter of the material, respectively. As shown in Fig. 2, due to much smaller effective particle diameter of cp-ESB powders than ss-ESB powers, the specific surface area of cp-ESB is much higher than ss-ESB. Therefore, co-precipitation successfully reduced the ESB particle size and significantly enlarged surface area, which should result in much higher sinterability.

3.2. Effect of sintering temperature on ESB/GDC bilayered electrolyte

In order to investigate the effect of particle size and sintering temperature on ESB layer formation, ESB/GDC bilayered electrolytes were fabricated using cp-ESB and ss-ESB powders at various sintering temperatures (700, 800, and 900 °C). The SEM images in Fig. 3 show cross-sectional views of the bilayered structures on anode supports. Using backscatter imagery, the different phases – ESB (white), GDC (light gray), and NiO (dark gray) – are easily distinguished due to differences in elemental contrast. It should be noted that the SEM images for each ESB layer (Fig. 3a, c, e, and g for ss-ESB and Fig. 3b, d, f, and h for cp-ESB) were taken at different magnifications.

From these microstructures, it is clear that both cp- and ss-ESB layers increase in density with increasing sintering temperature. However, the ESB layer prepared from the ss-ESB powder and fired at 900 °C (Fig. 3g) is not fully dense, rather it looks less dense than when fired at 800 °C (Fig. 3e) due to the formation of large pores. The melting temperature of Bi_2O_3 is ~825 °C [18]; however, stabilized bismuth oxides have much higher melting temperature, and differential thermal analysis (DTA) indicates no melting endotherm up to 1100 °C [19]. Therefore, we believe the decreasing density at higher temperature sintering is caused by Bi_2O_3 sublimation.

Moreover, the ESB layers are sintered on highly densified GDC sublayers that were previously sintered at a much higher temperature (~1450 °C). Therefore, the ESB sintering mechanism is accommodated by vertical shrinkage without lateral shrinkage. As a result, ss-ESB powder does not establish a dense layer due to its low surface area and large hard particle morphology leading to low sinterability. The film porosity is further impacted by Bi_2O_3 sublimation. Thus, micron-sized ESB powders prepared by conventional solid state synthesis are not appropriate for colloidal deposition of the ESB layer in ESB/GDC bilayered electrolytes.

On the other hand, as shown in Fig. 3b, d, f, and h, when cp-ESB powder was used, the ESB layer was highly dense when fired at 800 °C. SEM analysis (Fig. 2a), of the cp-ESB powder shows that it has a very high surface area due to the nano-sized nature of the particles. Therefore, it is possible for cp-ESB powder to produce sufficient surface energy at lower sintering temperatures for the particles to neck and densify by surface and lattice diffusion. Unlike the layer prepared from ss-ESB powder, the cp-ESB layer sintered at 900 °C (Fig. 3h) looks very dense. However the ESB thickness was reduced compared to the same layer sintered at 800 °C (Fig. 3f). Since 900 °C is above the pure Bi_2O_3 melting temperature, as discussed above, this indicates that partial sublimation of Bi_2O_3 and/or penetration of it into the GDC layer have possibly occurred.

It should be noted that as seen in Fig. 3g and h, both ss- and cp-ESB layers sintered at 900 °C show diffusion of ESB phase into ceria layer and segregation along GDC grain boundaries. This is also clearly shown in Fig. 4, which is a magnified image of Fig. 3g. This indicates that above the Bi_2O_3 melting temperature the higher activity of bismuth oxide (or bismuth in the ESB lattice) leads to

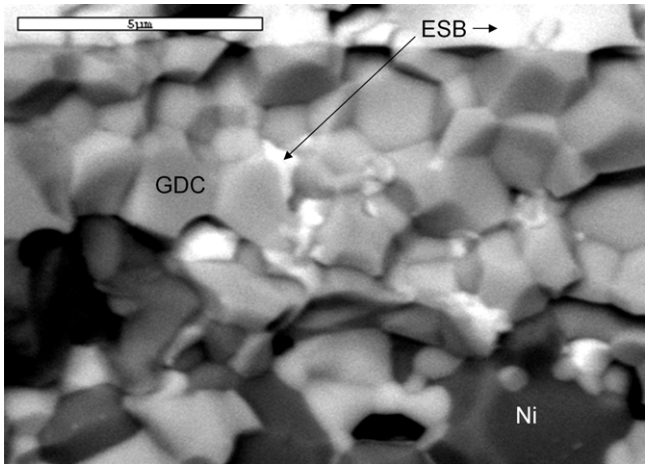

Fig. 4. Cross-sectional view of GDC electrolyte under ss-ESB layer after sintering at 900 °C, which is the magnified image from Fig. 3 g. In backscattering mode, ESB (white), GDC (light gray), and NiO (dark gray) phases are well-distinguishable, showing ESB penetration into GDC grain boundaries.

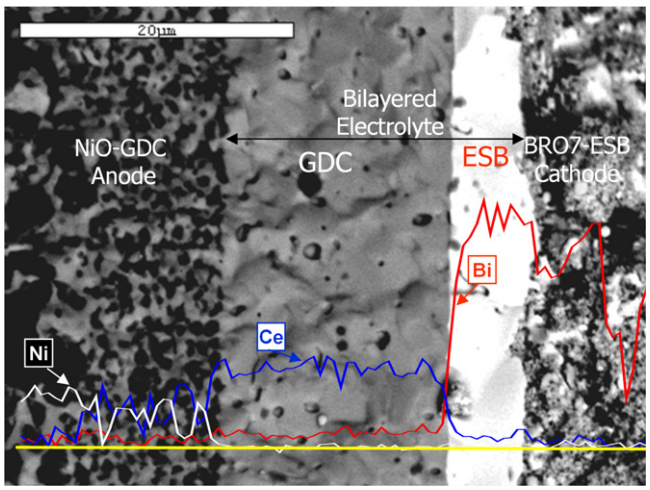

Fig. 5. Cross-sectional SEM image of a full button cell with ESB/GDC bilayered electrolyte. EDX line scan was conducted along the straight base line (yellow) and the intensity of each elements are presented as red (Bi), blue (Ce), and white (Ni) lines. (For interpretation of the references to color in this figure legend, the reader is referred to the web version of the article.)

diffusion along the GDC grain boundaries, which generally has a high surface energy. It has also been reported that bismuth oxide is soluble in CeO_2 forming a solid solution of $Bi_{1-x}Ce_xO_{2-x/2}$ with a cubic fluorite structure [20]. Gil et al. recently reported that the solid solubility limit of bismuth oxide in doped ceria is ~0.8 wt% [21]. Park et al. predicted the possible existence of solid solutioning at the interface between the stabilized bismuth oxide and doped ceria bilayered electrolytes [8]. In that study, the conductance was actually increased by adding a ~0.2 μm ESB layer on top of a 2 mm thick Sm doped ceria (SDC) as compared to a 2 mm SDC electrolyte alone. This phenomenon was explained by the formation of bismuth oxide in the SDC grain boundaries, which can lower the activation energy for oxygen ion transfer by scavenging grain boundary impurity phases. Therefore, while this indicates an apparent upper sintering temperature of <900 °C, it is not due to deleterious phase formation and may in fact have a positive effect on lowering ohmic polarization in the observed integrated ESB/GDC structure.

On the other hand, it was also found that the fracture mode of the GDC electrolyte with ESB sintered at 900 °C changed from intra-granular to inter-granular (Fig. 4) compared to GDC cross-sections near ESB layers sintered at lower temperature (Fig. 3a–f). This might cause deterioration in the mechanical strength of the GDC electrolyte due to highly segregated bismuth oxide along the GDC grain boundary. Therefore, this phenomenon should be carefully controlled and further investigation is needed.

Finally, Fig. 5 shows the cross-sectional SEM image of a complete SOFC consisting of NiO–GDC anode/ESB–GDC bilayered electrolyte/BRO7–ESB composite cathode. The ESB film was prepared by the colloidal deposition using cp-ESB and sintered at 800 °C. As shown in this figure, a dense ESB/GDC layer was obtained and every layer is clearly distinguishable with good interfacial contact. To examine the possible interdiffusion between layers, an energy dispersed X-ray (EDX) line scan analysis was conducted along the base line (yellow) in Fig. 5. Three elements were traced along the line, which includes Bi (red line), Ce (blue line), and Ni (white line). The resultant data are overlapped in Fig. 5 and no solid state reaction or interdiffusion between layers was observed.

These results demonstrate that we can obtain dense ESB/GDC bilayered electrolytes by a simple colloidal deposition process using fine ESB powders made by co-precipitation. The optimal sintering temperature is ~800 °C, which limits Bi_2O_3 sublimation and penetration into the GDC electrolyte.

3.3. Effect of thickness of ESB/GDC bilayered electrolyte on OCP

For comparison of electrochemical performance, four electrolytes were prepared, including three different thicknesses of GDC/ESB bilayered electrolytes and one single GDC electrolyte as a reference. To control overall electrolyte thickness, the colloidal deposition process of ESB was repeated until the desired thickness was attained. The cross-sectional views of the samples were observed by SEM. Fig. 6 shows the cross-sectional views of the GDC/ESB bilayered and GDC single layered fuel cells. The samples are referred to as 48GDC4ESB, 16GDC6ESB, 10GDC5ESB, and 10GDC where the number refers to the layer thickness in μm. For all bilayered electrolytes the thickness of the ESB layer are similar ~5 μm. Moreover, both GDC and ESB layers are very dense with a few closed pores and the ESB layers are well bonded with the GDC layers as shown in inset of Fig. 6d.

OCP measurements for each cell were conducted with 30 sccm of dry air and 30 sccm of H_2 (3% wet) on the cathode and the anode side, respectively, over the temperature range 500–650 °C. The resultant OCPs are plotted in Fig. 7. The 10GDC5ESB bilayer electrolyte cell shows a significant OCP enhancement compared to the ~10 μm thick GDC single layer electrolyte for all temperatures. This result indicates that the thin ~5 μm ESB layer decreased the electronic conduction through the GDC electrolyte, caused by reduction of Ce^{4+} to Ce^{3+}. It is also noted that the OCP increase from 0.72 V (10GDC) to 0.78 V (10GDC5ESB) at 650 °C is in good agreement with our previous results of 0.77 V with a 10GDC/4ESB bilayered electrolyte deposited by PLD [13]. This demonstrates both reproducibility of results and that thin and dense ESB/GDC bilayered electrolytes can be achieved by conventional colloidal process using our nano-sized ESB powder.

OCP also increases with increasing GDC layer thickness for ESB/GDC bilayer electrolytes as shown in Fig. 7. For example, the OCPs at 650 °C were 0.78, 0.84, and 0.88 V for 10GDC5ESB, 16GDC6ESB, and 48GDC4ESB, respectively. This is consistent with our previous continuum analytical modeling of MIECs, such as doped-ceria, due to a decrease in leakage current and oxygen ion permeability with increasing MIEC electrolyte thickness resulting in an increase in OCP [22]. More recently, we experimentally confirmed the dependence of MIEC electrolyte thickness on OCP [23].

However, it should be noted that thinner electrolytes are desirable to reduce ohmic polarization. In addition, increasing the

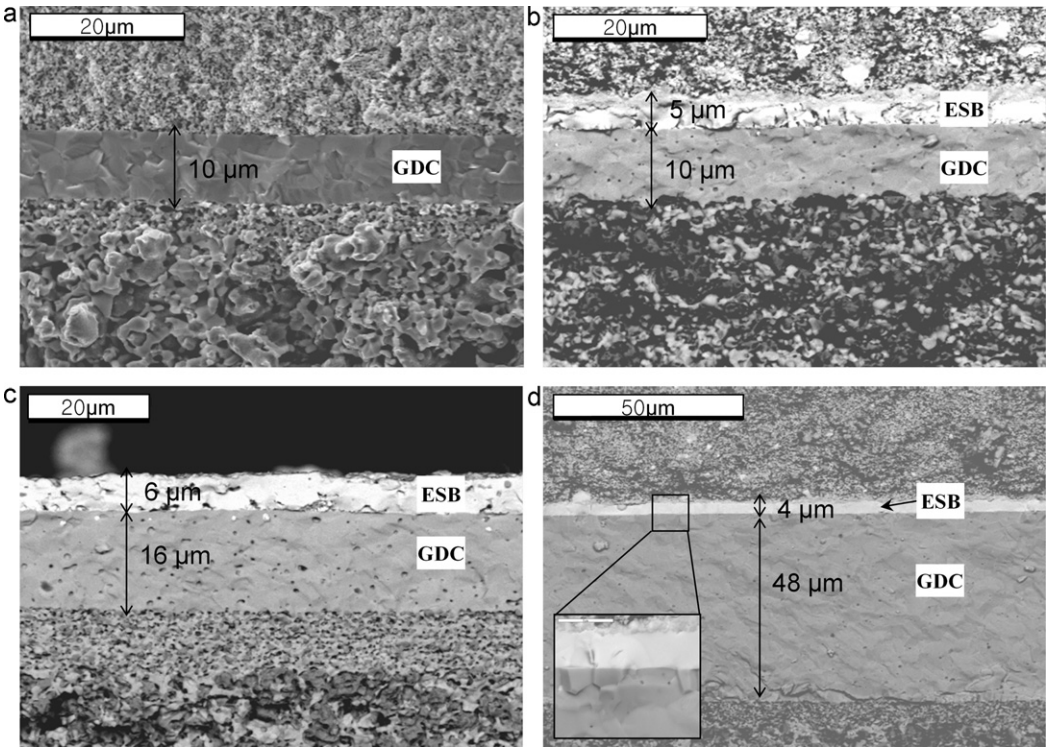

Fig. 6. SEM images of cross-sectional views of a single GDC electrolyte cell (a) and ESB/GDC bilayered cells with various thicknesses (b–d). The magnified view of GDC/ESB interface is inset in (d) (images used in [26]).

relative ESB to GDC thickness ratio of the bilayer electrolyte increases the effective transference number and OCP [9]. Moreover, using a greater ESB/GDC thickness ratio lowers the ohmic ASR due to the order of magnitude higher ionic conductivity of ESB compared to that of GDC. Thus, further study of the optimization of total and relative thickness of the ESB/GDC bilayered electrolytes is warranted.

3.4. Performance of a button cell with ESB/GDC bilayered electrolyte

The *I–V* characteristics of SOFCs with a GDC single layer (10GDC) and an ESB/GDC bilayered electrolyte (10GDC5ESB), at 650 °C with 90 sccm H_2 (3% wet) anode side and 30 sccm dry air cathode side, are shown in Fig. 8a. The maximum power density (MPD) of the bilayered electrolyte reached ~1.47 W cm^{-2}. This is a 69% increase in MPD compared to 10GDC (~0.87 W cm^{-2}). The OCPs of the

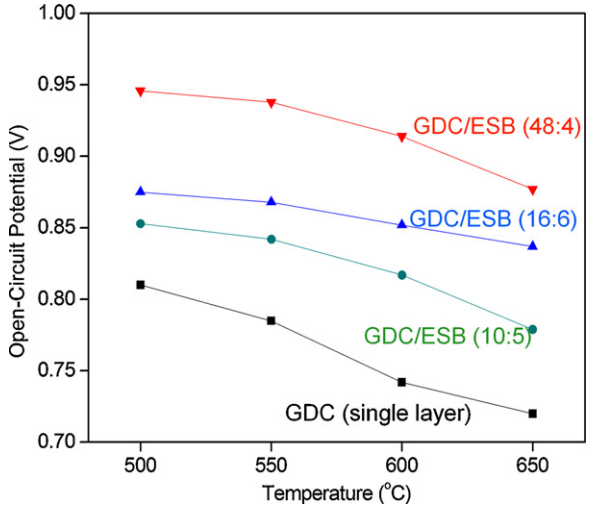

Fig. 7. OCP measurement result of GDC/ESB bilayers with various thicknesses and a single GDC layer on OCP at the temperature ranges from 500 to 650 °C (image used in [26]).

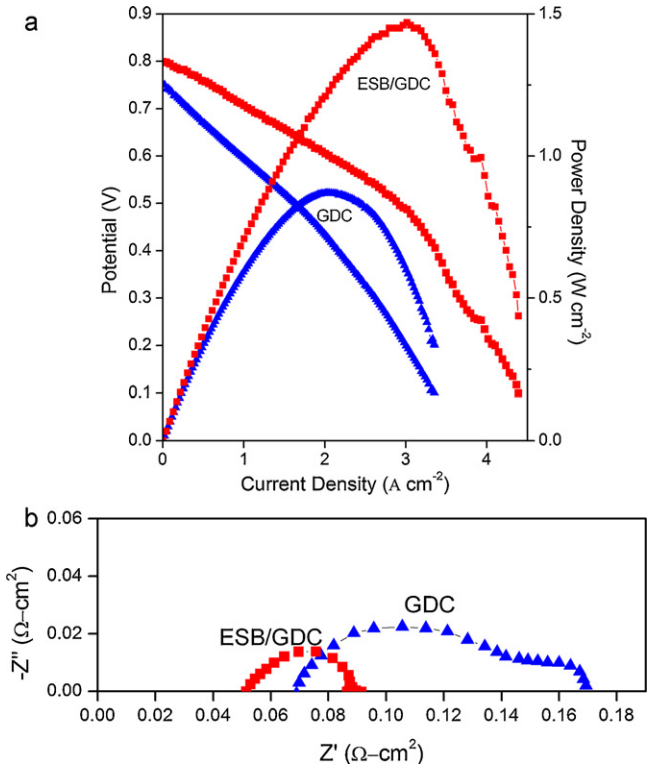

Fig. 8. Current–voltage (*I–V*) and current–power (*I–P*) curves (a), and impedance spectra (b) of ESB/GDC bilayer (red square) and GDC single layer (blue triangle) cell at 650 °C. (For interpretation of the references to color in this figure legend, the reader is referred to the web version of the article.)

Table 2
Summary of electrochemical performance of the studied cells.

Cell Type	GDC thickness (μm)	ESB thickness (μm)	OCP (V)	MPD (W cm^{-2})	Total ASR$_{IV}$ (Ω cm^2)	Total ASR$_{EIS}$ (Ω cm^2)	Ohmic ASR (Ω cm^2)	Electrode ASR (Ω cm^2)	Ref.
10GDC	10	–	0.75	0.87	0.164	0.168	0.069	0.099	This study
10GDC/5ESB	10	5	0.80	1.47	0.084	0.088	0.051	0.037	This study
GDC/PLD–ESB	10	4	0.77	1.94	0.075	0.079	0.046	0.033	[13]

10GDC and 10GDC5ESB SOFCs were 0.75 and 0.80 V, respectively. These are somewhat higher values compared to the OCP measurements in Section 3.4 (although the differential between single layer and bilayer is essentially the same) and are most likely due to the increased H_2 flow (from 30 sccm to 90 sccm). While the bilayered electrolyte resulted in a ~0.05 V increase in OCP, the major enhancement in MPD came from the ASR reduction. The estimated total ASRs from IV curves near OCP were 0.084 Ω cm^2 and 0.164 Ω cm^2 for 10GDC5ESB and 10GDC, respectively.

Further analysis by electrochemical impedance was conducted (Fig. 8b). In these Nyquist plots the total and ohmic ASR were extracted from the low and high frequency intercepts of the impedance spectra with the real axis, respectively, and the electrode ASR was calculated from the difference between these two ASR values. The detailed values are shown in Table 2. The total ASR of the 10GDC5ESB bilayer cell (0.088 Ω cm^2) decreased by 47.6% compared to that of the 10GDC cell (0.168 Ω cm^2). The total ASRs from these AC impedance tests are identical to the ASRs from the *I–V* curves (DC impedances) within 5% deviation showing validity of results.

The electrode ASR of the 10GDC5ESB bilayer cell decreased by 62.6% compared to that of the 10GDC cell. This ASR drop (0.062 Ω cm^2) is believed to come from the cathodic polarization reduction at the interface between BRO7–ESB cathode and ESB electrolyte, considering that both cells utilized the same GDC layer, anode material, and identical procedures. This interpretation is well-supported by our former studies [12,14].

The ohmic ASR also decreased with the addition of the ESB layer (26.1%, 0.018 Ω cm^2) at 650 °C. In theory, the ohmic ASR ($ASR_{electrolyte}$) of a bilyared electrolyte can be estimated by simply modeling two series resistors:

$$ASR_{electrolyte} = L_{GDC}\left(\frac{\tau}{\sigma_{ESB}} + \frac{1}{\sigma_{GDC}}\right) \quad (3)$$

where L_{GDC} is thickness of GDC electrolyte, τ is thickness ratio of ESB to GDC, and σ_{ESB} and σ_{GDC} are the conductivities of ESB and GDC, respectively [14,24]. Based on known ESB and GDC conductivities [25], a similar or slightly higher ohmic ASR of the 10GDC5ESB bilayered electrolyte than that of a single 10GDC is expected by Eq. (3). However, our studies repeatedly show that ESB/GDC bilayer electrolytes effectively reduce the electrolyte ASR even when we add an additional ESB layer on top of the same thickness GDC layer [9,13,14]. Therefore, we believe this is due to reduction in the GDC grain boundary resistance by penetration and segregation of Bi_2O_3 to the GDC grain boundaries, even when it is not detectable in EDX analysis.

The current MPD results for this ESB/GDC bilayer cell are somewhat lower than we previously reported MPD (~1.95 W cm^{-2}) with similar thicknesses of ESB (by PLD) and GDC (Table 2) [13]. This is most likely because in this study we used both solid-state BRO7 and ESB powders for the cathode, while in the previous study we used a microstructurally optimized BRO7–ESB cathode, as described in detail by Camaratta and Wachsman [12]. Therefore, we expect higher MPD is achievable by further improvement of ESB/GDC thicknesses and use of optimized cathodes.

4. Conclusion

We fabricated thin and dense ESB/GDC bilayered electrolytes by a simple colloidal deposition process. A wet chemical co-precipitation route was used to produce highly sinterable nano-ESB particles. Dense and thin (~5 μm) ESB layers were established on GDC electrolyte by simple colloidal drop coating using this nano-scale ESB powder. The optimal sintering temperature of the ESB layer was found to be ~800 °C due to its poor densification at lower temperatures and solid state diffusion and sublimation at higher temperatures. We demonstrated an increase in OCP by addition of the ESB layer, as well as by the thickness of the constituent GDC layer, in ESB/GDC bilayer electrolytes.

Finally, an anode-supported ESB/GDC bilayered electrolyte SOFC coupled to a BRO7–ESB cathode produced a high maximum power density of ~1.5 W cm^{-2} at 650 °C. This was achieved due to the effect of the bilayered electrolyte on increasing OCP and decreasing both electrode ASR and ohmic ASR. Moreover, this study demonstrates the feasibility of high performance low temperature ESB/GDC bilayered electrolyte SOFCs by cost-effective and scalable colloidal deposition techniques.

Acknowledgments

This work was supported by the Office of Naval Research (Contract No. N00014-09-C-0467). Also, Kang Taek Lee acknowledges the Kwanjeong educational foundation scholarship.

References

[1] N.Q. Minh, J. Am. Ceram. Soc. 76 (1993) 563–588.
[2] B.C.H. Steele, J. Mater. Sci. 36 (2001) 1053–1068.
[3] B.C.H. Steele, Solid State Ionics 129 (2000) 95–110.
[4] H. Inaba, H. Tagawa, Solid State Ionics 83 (1996) 1–16.
[5] K. Eguchi, T. Setoguchi, T. Inoue, H. Arai, Solid State Ionics 52 (1992) 165–172.
[6] E.D. Wachsman, G.R. Ball, N. Jiang, D.A. Stevenson, Solid State Ionics 52 (1992) 213–218.
[7] E.D. Wachsman, P. Jayaweera, N. Jiang, D.M. Lowe, B.G. Pound, J. Electrochem. Soc. 144 (1997) 233–236.
[8] J.Y. Park, H. Yoon, E.D. Wachsman, J. Am. Ceram. Soc. 88 (2005) 2402–2408.
[9] J.Y. Park, E.D. Wachsman, Ionics 12 (2006) 15–20.
[10] Y.J. Leng, S.H. Chan, Electrochem. Solid State Lett. 9 (2006) A56–A59.
[11] A. Jaiswal, C.T. Hu, E.D. Wachsman, J. Electrochem. Soc. 154 (2007) B1088–B1094.
[12] M. Camaratta, E. Wachsman, J. Electrochem. Soc. 155 (2008) B135–B142.
[13] J.S. Ahn, D. Pergolesi, M.A. Camaratta, H. Yoon, B.W. Lee, K.T. Lee, D.W. Jung, E. Traversa, E.D. Wachsman, Electrochem. Commun. 11 (2009) 1504–1507.
[14] J.S. Ahn, M.A. Camaratta, D. Pergolesi, K.T. Lee, H. Yoon, B.W. Lee, D.W. Jung, E. Traversa, E.D. Wachsman, J. Electrochem. Soc. 157 (2010) B376–B382.
[15] J.S. Ahn, H. Yoon, K.T. Lee, M.A. Camaratta, E.D. Wachsman, Fuel Cells 9 (2009) 643–649.
[16] D.W. Jung, K.L. Duncan, M.A. Camaratta, K.T. Lee, J.C. Nino, E.D. Wachsman, J. Am. Ceram. Soc. 93 (2010) 1384–1391.
[17] A.L. Patterson, Phys. Rev. 56 (1939) 978–982.
[18] T. Takahashi, T. Esaka, H. Iwahara, J. Solid State Chem. 16 (1976) 317–323.
[19] N.X. Jiang, E.D. Wachsman, J. Am. Ceram. Soc. 82 (1999) 3057–3064.
[20] M. Hrovat, A. Bencan, J. Holc, T. Rojac, M. Kosec, J. Mater. Res. 18 (2003) 1297–1300.
[21] V. Gil, J. Tartaj, C. Moure, P. Duran, Ceram. Int. 33 (2007) 471–475.
[22] K.L. Duncan, E.D. Wachsman, J. Electrochem. Soc. 156 (2009) B1030–B1038.
[23] K.L. Duncan, K.T. Lee, E.D. Wachsman, J. Power Sources 196 (2011) 2445–2451.
[24] E.D. Wachsman, Solid State Ionics 152 (2002) 657–662.
[25] D.W. Jung, K.L. Duncan, E.D. Wachsman, Acta Mater. 58 (2010) 355–363.
[26] E. Wachsman, K.T. Lee, Science 334 (2011) 935–939.